

Giant Valley-Zeeman Splitting from Spin-Singlet and Spin-Triplet Interlayer Excitons in $WSe_2/MoSe_2$ Heterostructure

Tianmeng Wang^{1#}, Shengnan Miao^{1#}, Zhipeng Li^{1#}, Yuze Meng^{1#}, Zhengguang Lu^{2,3}, Zhen Lian¹, Mark Blei⁴, Takashi Taniguchi⁵, Kenji Watanabe⁵, Sefaattin Tongay^{4*}, Dmitry Smirnov², Su-Fei Shi^{1,6*}

1. Department of Chemical and Biological Engineering, Rensselaer Polytechnic Institute, Troy, NY 12180, USA
2. National High Magnetic Field Lab, Tallahassee, FL, 32310
3. Department of Physics, Florida State University, Tallahassee, Florida 32306, USA
4. School for Engineering of Matter, Transport and Energy, Arizona State University, Tempe, AZ 85287, USA
5. National Institute for Materials Science, 1-1 Namiki, Tsukuba 305-0044, Japan.
6. Department of Electrical, Computer & Systems Engineering, Rensselaer Polytechnic Institute, Troy, NY 12180, USA

These authors contributed equally to this work

* Corresponding authors: shis2@rpi.edu, Sefaattin.Tongay@asu.edu

ABSTRACT

Transition metal dichalcogenides (TMDCs) heterostructure with a type II alignment hosts unique interlayer excitons with the possibility of spin-triplet and spin-singlet states. However, the associated spectroscopy signatures remain elusive, strongly hindering the understanding of the Moiré potential modulation of the interlayer exciton. In this work, we unambiguously identify the spin-singlet and spin-triplet interlayer excitons in the $WSe_2/MoSe_2$ hetero-bilayer with a 60-degree twist angle through the gate- and magnetic field-dependent photoluminescence spectroscopy. Both the singlet and triplet interlayer excitons show giant valley-Zeeman splitting between the K and K' valleys, a result of the large Landé g-factor of the singlet interlayer exciton and triplet interlayer exciton, which are experimentally determined to be ~ 10.7 and ~ 15.2 , respectively, in good agreement with theoretical expectation. The PL from the singlet and triplet interlayer excitons show opposite helicities, determined by the atomic registry. Helicity-resolved photoluminescence excitation (PLE) spectroscopy study shows that both singlet and triplet interlayer excitons are highly valley-polarized at the resonant excitation, with the valley polarization of the singlet interlayer exciton approaches unity at ~ 20 K. The highly valley-polarized singlet and triplet interlayer excitons with giant valley-Zeeman splitting inspire future applications in spintronics and valleytronics.

KEYWORDS: *interlayer exciton, singlet, triplet, valley polarization, Zeeman shift*

Due to the reduced screening in two-dimension (2D), the enhanced Coulomb interaction not only gives rise to strongly bound exciton in monolayer TMDC¹⁻⁶ but also leads to robust interlayer exciton in a TMDC hetero-bilayer of the type II alignment, with the optically excited electron and hole residing in different TMDC layers⁷⁻¹⁶. The spatial separation of the electron and hole results in the long lifetime of the interlayer exciton¹⁷⁻²². It was also theoretically predicted that the TMDC hetero-bilayer would host interlayer exciton fine structures: singlet and triplet interlayer excitons²³, a result of the spin-orbit coupling induced splitting of the conduction bands for monolayer TMDCs²⁴⁻³¹. Interestingly, the triplet interlayer exciton, unlike its counterpart in monolayer TMDC^{32,33}, is not restricted by the mirror symmetry and could have finite radiation through the in-plane dipole, depending on the atomic registry of the hetero-bilayer²³. The long-lived singlet and triplet interlayer excitons could also retain valley polarization³⁴⁻⁴⁰, promising for valleytronics applications.

Interestingly, the small twist angle or lattice mismatch between the TMDCs hetero-bilayer would generate a Moiré superlattice potential⁴¹⁻⁴⁴, which modulates the interlayer exciton and leads to more fine features. The Moiré modulated interlayer exciton complicates the optical spectra^{45,46} and renders it even more challenging to identify the triplet and singlet interlayer excitons. On the other side, identification of the singlet and triplet interlayer excitons would be critical for exploring Moiré potential to engineer interlayer exciton. In this work, we construct a perfectly aligned WSe₂/MoSe₂ heterostructure with a 60-degree twist angle. We unambiguously identify the singlet and triplet interlayer excitons through gate-, temperature-, and magnetic field-dependent photoluminescence (PL) spectroscopy. We found that both the singlet and triplet interlayer excitons have a large response to the out-of-plane magnetic field, with the Landé g-factor as large as ~ 10.7 and ~ 15.2, respectively, in excellent agreement with theoretical expectation^{47,48}. These g-factors are much larger than that of the bright intralayer exciton in monolayer TMDC (~ 4)^{6,49} and lead to a giant valley-Zeeman splitting between the K and K' valleys⁵⁰, ~ 11.2 meV and ~ 16.0 meV for the singlet and triplet interlayer excitons, respectively, for an out-of-plane magnetic field of 17.5 T.

We also find that the singlet and triplet interlayer excitons possess opposite valley polarization, corresponding to a H_h^h atomic registry predicted theoretically²³. The helicity-resolved photoluminescence excitation (PLE) spectroscopy study shows that the PL from each interlayer exciton is highly valley polarized at resonance excitation, which for singlet interlayer exciton can be as high as ~ -100% at 23 K and ~ -85% even for the elevated temperature of 82 K. The high valley polarization of the interlayer excitons originates from the long valley lifetime of the holes⁵¹⁻⁵³. The robust valley polarization of the long-lived interlayer excitons thus presents new quasiparticles for valleytronics applications, while the giant valley-Zeeman splitting could be further exploited to break the valley degeneracy.

The monolayer MoSe₂ and WSe₂ were exfoliated separately, with the crystal orientation determined by the second harmonic generation (SHG). The twist angle between the constructed hetero-bilayer was further determined to be 60 degrees by comparing the

SHG signals from the heterostructure region and monolayer region (see SI). The heterostructure was further encapsulated with few-layer boron nitride (BN) flakes and integrated into the dual gated device using a similar method as described previously^{6,49,54}. The schematic of constructed heterostructure device is shown in Fig. 1a, and a typical device image is shown in Fig. 1b. At 77 K, the PL spectra of one device (Fig. 1c) show much quenched PL of intralayer bright exciton of MoSe₂ and WSe₂, at 1.624 eV and 1.706 eV respectively, while two pronounced interlayer exciton-PL peaks centered at 1.392 eV and 1.416 eV. These two peaks can be tuned by the gate voltage. As shown in Fig. 1d and 1e, when the gate voltage is positive, which corresponds to the electron doping of the bottom layer, the two peaks exhibit a sensitive shift as a function of the top gate voltage due to the Stark shift^{54,55}. It is worth noting that, for a device which we place MoSe₂ as the bottom layer (Fig. 1d), we observe a blue-shift of the two peaks, opposite to the red-shift observed in the device with the opposite hetero-bilayer stacking order (Fig. 1e), confirming that the observed two PL peaks are associated with the interlayer exciton, whose dipole direction switches as the stacking order switches.

To reveal the nature of the observed two PL peaks associated with the interlayer exciton, we performed a magnetic field dependent PL spectroscopy study. We use a linearly polarized continuous wave (CW) laser centered at 1.959 eV as the excitation, and the obtained PL spectra as a function of the out-of-plane magnetic field are shown as a color plot in Fig. 2a. It is evident that, in the presence of the magnetic field, each of the PL peaks is split into two, with the splitting as large as ~16.0 meV for the triplet interlayer exciton (IX_T) and ~11.2 meV for the singlet interlayer exciton (IX_S) under the magnetic field of 17 T. This splitting is due to the valley-Zeeman shift since the linearly polarized light excites both K and K' valleys, which undergoes an opposite shift in the presence of the out-of-plane magnetic field²⁶⁻²⁹. This splitting can be expressed as $\Delta E = g\mu_B B$, in which g is the Landé g -factor, μ_B is the Bohr magneton, and B is the magnetic field strength. As shown in Fig. 2b, the experimentally measured energy splitting for different magnetic field strengths can be fitted with a linear function, which gives the g factor ~ 15.2 for IX_T and ~ 10.7 for IX_S. These g factors are much larger than that of the bright exciton or trions in monolayer TMDC (~ 4)^{6,49,56,57}, attributing to the giant valley-Zeeman splitting of the interlayer excitons⁵⁸.

The measured g -factor can also be used to determine the nature of the interlayer exciton peaks. As shown by recent studies, the spin-orbit coupling in monolayer TMDC not only leads to a large splitting of the valence bands (300-500 meV) but also gives rise to a splitting in the conduction bands, which is much smaller in scale (~ 20 meV)^{59,60}. As a result, for the WSe₂/MoSe₂ heterostructure with a 60-degree twist angle, the K valley of WSe₂ is aligned with the K' valley of MoSe₂, as schematically shown in Fig. 2c, d. It has been shown previously that the conduction band splitting gives rise to the spin triplet exciton, aka spin-dark exciton, in monolayer TMDCs^{32,33,58}. Here, the presence of the conduction band splitting renders it possible to have two configurations of the interlayer exciton: spin triplet (IX_T) and spin singlet (IX_S) interlayer exciton, as shown in Fig. 2d. At a finite temperature, the thermal fluctuation ensures a certain population of exciton in the

higher energy IX_S , and both peaks are clearly visible in the PL spectra (Fig. 1d-e and Fig. 2a). In a non-interacting picture, the g factor for either of the interlayer exciton, IX_T or IX_S , can be calculated theoretically counting the overall contribution of the spin, orbital and valley components, and it is expected to be 16 for IX_T and 12 for IX_S (see SI). The experimentally extracted values are in excellent agreement with the theoretical expectations, confirming the assignment of the singlet and triplet interlayer excitons. It is worth noting that, in monolayer WSe_2 or WS_2 , the triplet exciton is a spin-forbidden dark exciton and can only radiate through an out-of-plane dipole^{6,31,49,61–65}. In the $WSe_2/MoSe_2$ heterostructure that we investigate here, due to the lift of the out-of-plane mirror symmetry, the triplet interlayer exciton is not necessarily dark and could have significant in-plane dipole radiation. The recent theory has shown that, depending on the exact atomic registry of the hetero-bilayers, there could be significant in-plane dipole radiation with valley information retained²³.

To investigate the valley polarization of the interlayer excitons, we perform helicity resolved PLE spectroscopy study. We first excite the heterostructure with circularly polarized light (σ^+) with different the excitation photon energies, and we detect the PL with the same (σ^+) or opposite helicity (σ^-). The obtained data near the interlayer exciton energy (from 1.355 eV to 1.470 eV) at 77 K is shown in Fig. 3a. It is evident that the PL intensity is at its local maximum when the excitation is in resonance with the A or B exciton of either $MoSe_2$ (X_A^{Mo} , X_B^{Mo}) or WSe_2 (X_A^W , X_B^W). More interestingly, at resonant excitation, the relative intensity of the IX_S and IX_T in different detection schemes are significantly different, as shown in Fig. 2d. For the excitation photon energy (1.722 eV) in resonance with the A exciton of the WSe_2 , the higher PL intensity peak of IX_T in the $\sigma^+\sigma^+$ detection scheme switches to the lower intensity in the $\sigma^+\sigma^-$ configuration. Similarly to the definition of the intralayer bright exciton in monolayer TMDC, we define valley polarization as $P = \frac{I(\sigma^+) - I(\sigma^-)}{I(\sigma^+) + I(\sigma^-)}$, in which $I(\sigma^+)$ is the integrated PL intensity of the same helicity (σ^+) and $I(\sigma^-)$ is the integrated PL intensity of the opposite helicity (σ^-). The switch of the relative PL intensity is due to the negative valley polarization of the IX_S and positive valley polarization of the IX_T (Fig. 3b). The particular helicity of PL emission agrees with the H_h^h atomic registry (see SI Section S7)²³, in which the singlet and triplet interlayer exciton both radiate through an in-plane dipole but with opposite helicity. As shown in Fig.3b, the valley polarization of the two interlayer excitons is sensitively dependent on the excitation photon energy. At the excitation photon energy of 1.722 eV, the valley polarization of the singlet interlayer exciton (IX_S) is as high as $\sim 32.9\%$ and the triplet interlayer exciton (IX_T) could be as high as $\sim -58.6\%$ at 77 K (Fig. 3d). When the excitation photon energy is off-resonance (2.138 eV in Fig. 3c), the valley polarization for both interlayer excitons vanishes.

The valley polarization also sensitively depends on the temperature. The temperature dependent PL spectra for the $\sigma^+\sigma^+$ and $\sigma^+\sigma^-$ configurations are shown in Fig. 4a and Fig. 4b, respectively. Fig. 4a shows that, as we detect the PL of the same helicity of the excitation light, the higher energy singlet interlayer exciton PL decreases significantly as

the temperature is decreased, suggesting that the singlet interlayer exciton is in thermal equilibrium with the triplet interlayer exciton and is thermally populated. The thermal equilibrium picture is also confirmed through lifetime measurements, which shows similar lifetime of the singlet and triplet interlayer exciton (see SI). In contrast, in the $\sigma^+\sigma^-$ scheme (Fig. 4b), as we detect the PL in the opposite helicity channel, the singlet interlayer exciton PL becomes pronounced at the lower temperature, which is due to the increased negative valley polarization and is shown explicitly in Fig. 4c. Fig. 4c plotted the valley polarization (P) of the triplet and singlet interlayer excitons as a function of the temperature at the resonant excitation of 1.722 eV (in resonance with the A exciton of WSe₂). As the temperature is decreased to 23 K, the valley polarization of the singlet interlayer exciton is approaching 100%. This high valley polarization arises from the long valley lifetime of the hole^{51–53}. The optically excited electron-hole pairs can quickly dissociate and separate into two layers^{66–69}, but the intervalley scattering of the hole is strongly inhibited^{34,50,51}, especially for resonance excitation^{35–40}. This sensitive temperature dependence of the valley polarization for both interlayer exciton can be easily illustrated in Fig. 4d, which shows PL spectra of the $\sigma^+\sigma^+$ and $\sigma^+\sigma^-$ configurations for temperatures of 42 K and 82 K.

Interestingly, the valley polarization of the triplet interlayer exciton seems to saturate at the temperature around 102 K, with a saturated value of $\sim 40\%$, less than that of the singlet interlayer exciton. We suspect that it is due to the lower energy nature of the triplet interlayer exciton, and the PL is more likely to be affected by defect PL at similar energy. This is supported by our observation in Fig. 4a, b, which shows that the PL near 1.395 eV is significantly broadened as the temperature is decreased.

In summary, we report the unambiguous identification of the triplet and singlet interlayer excitons through gate-, magnetic field-, and temperature-dependent PL spectroscopy study. The helicity resolved PLE spectroscopy study shows that the valley polarization of the interlayer exciton can approach unity at low temperature. These highly valley polarized interlayer excitons, with giant valley-Zeeman splitting, inspire future exploration of applications in valleytronics and spintronics. Utilization of the proximity field of a 2D magnetic material^{70–75} could take advantages of the large valley-Zeeman splitting in a device configuration, without the necessity of involving an external magnetic field.

Supporting Information

Details about sample preparation, optical characterization and data analysis can be found in the supporting information (SI).

Notes

The authors declare no competing financial interest.

ACKNOWLEDGMENTS

We thank Dr. Chenhao Jin for helpful discussions. T. Wang and S.-F. Shi acknowledge support from ACS PRF through grant 59957-DNI10. S. Miao, Z. Li and S.-F. Shi acknowledge support from AFOSR through Grant FA9550-18-1-0312. Z. Lian and S.-F. Shi acknowledge support from NYSTAR through Focus Center-NY–RPI Contract C150117. S. Tongay acknowledges support from NSF DMR-1552220, DMR-1838443, and CMMI-1933214. The device fabrication was supported by Micro and Nanofabrication Clean Room (MNCR) at Rensselaer Polytechnic Institute (RPI). K.W. and T.T. acknowledge support from the Elemental Strategy Initiative conducted by the MEXT, Japan and the CREST (JPMJCR15F3), JST. Z. Lu and D.S. acknowledge support from the US Department of Energy (DE-FG02-07ER46451) for magneto-photoluminescence measurements performed at the National High Magnetic Field Laboratory (NHMFL), which is supported by National Science Foundation through NSF/DMR-1644779 and the State of Florida. S.-F. Shi also acknowledges the support from a KIP grant from RPI and a VSP grant from NHMFL.

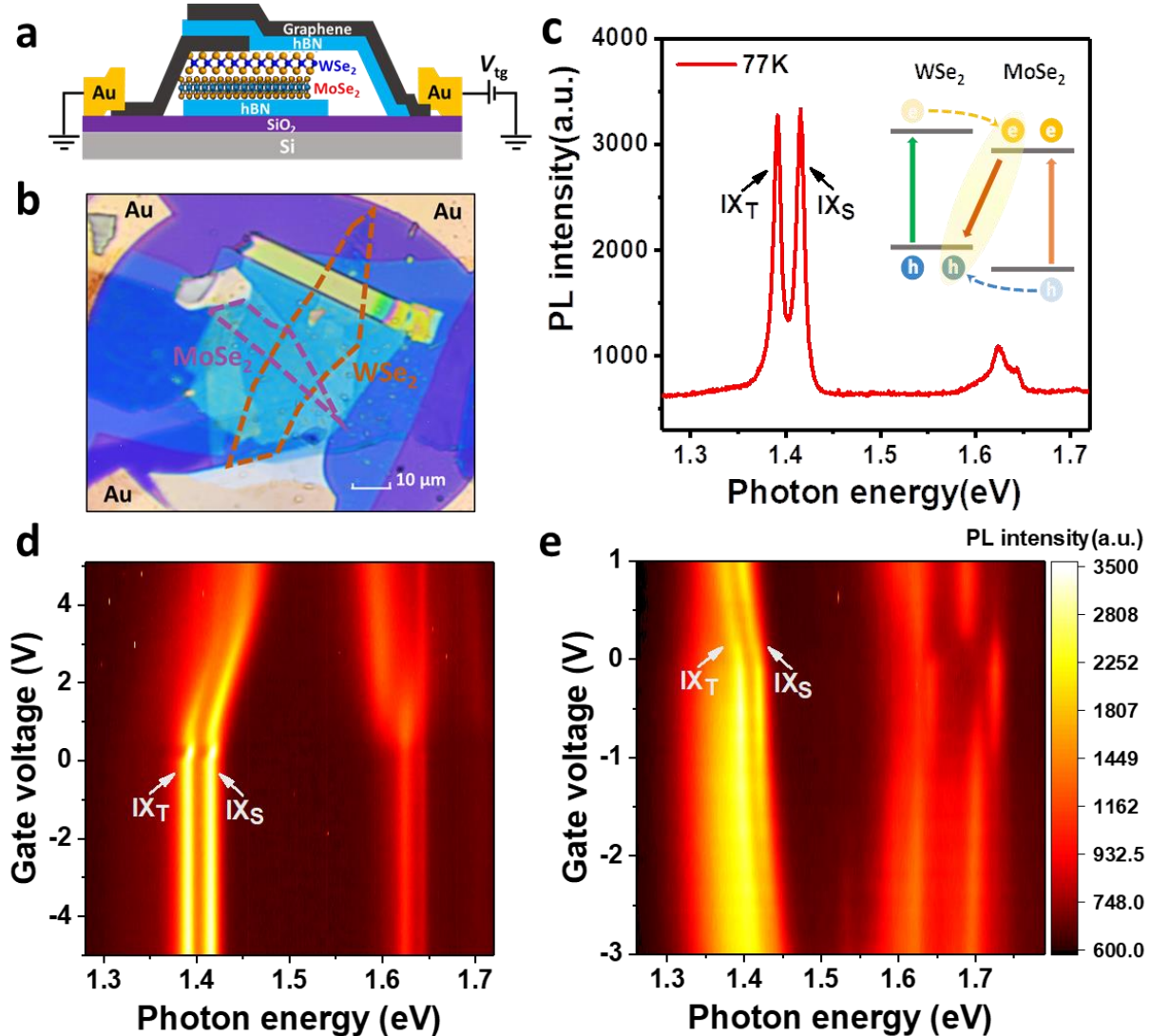


Figure 1. Interlayer excitons in WSe₂/MoSe₂ hetero-bilayer. (a) Schematic of the BN-encapsulated WSe₂/MoSe₂ heterostructure. One piece of few-layer graphene is used as the contact electrode and another piece is used as the transparent top-gate electrode. (b) Microscope image of the device. Scale bar: 10 μm. (c) PL spectra of the heterostructure, which exhibits two interlayer exciton peaks at 77 K. The CW laser centered at 1.959 eV was used as the excitation source. Inset: schematic of the type II band alignment of WSe₂/MoSe₂ hetero-bilayer. (d) Color plot of the PL spectra at 77 K of the WSe₂ (on top)/MoSe₂ heterostructure as a function of gate voltage, which is the same stacking sequence as the scheme in (a). (e) Color plot of the PL spectra at 77 K of the MoSe₂ (on

top)/WSe₂ heterostructure as a function of gate voltage, which is the opposite stacking sequence as the scheme in (a).

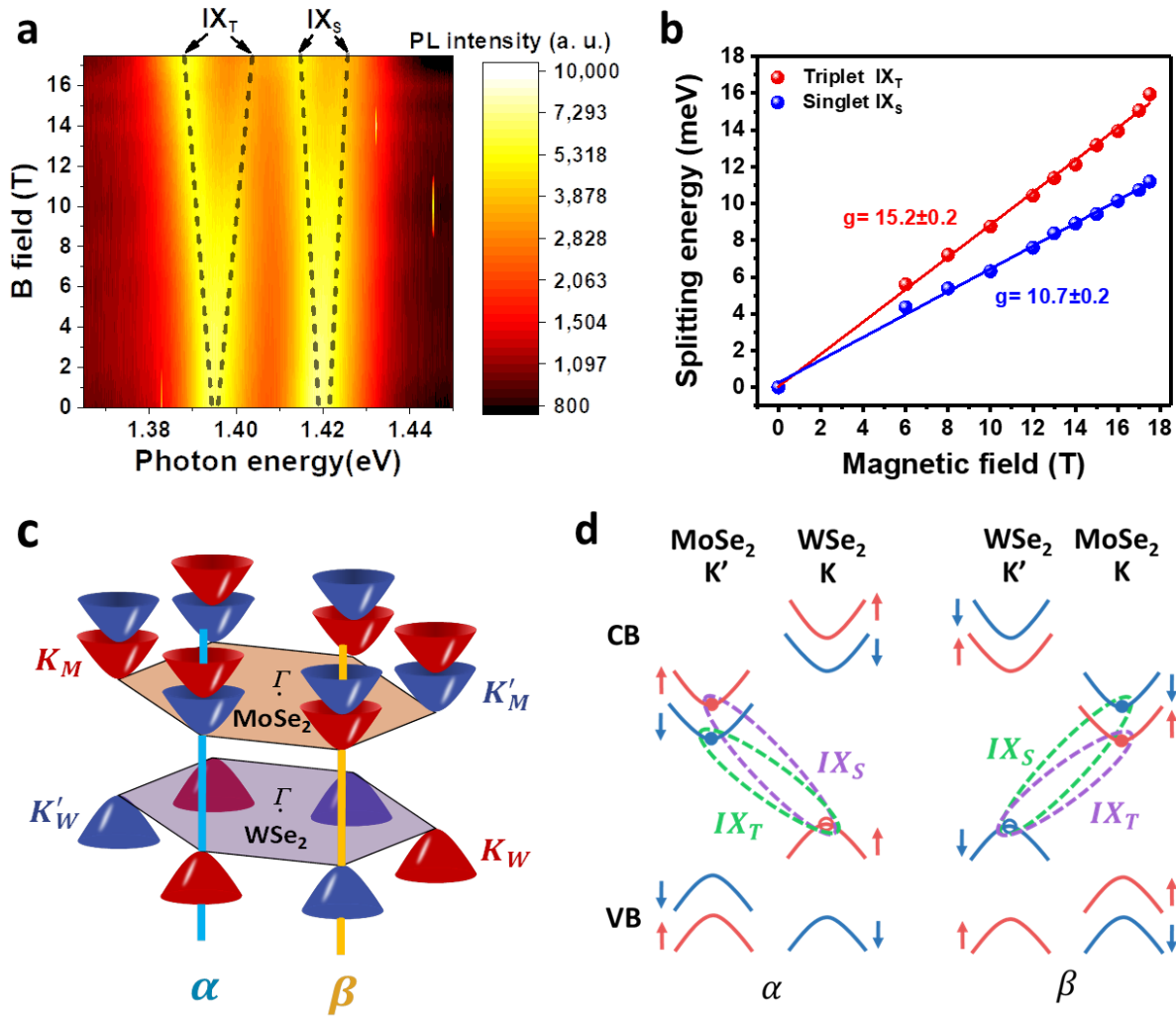


Figure 2. Magneto-PL spectra of interlayer excitons. (a) Color plot of the PL spectra of interlayer exciton as a function of the out-of-plane magnetic field at 77 K. The CW laser centered at 1.959 eV with a power of 250 μ W was used as the excitation source. (b) PL peak energy splitting for both interlayer exciton states. The valley-Zeeman splitting of each interlayer exciton is utilized to extract the corresponding g-factor through a linear fitting. (c) Illustration of the band structure at the corners (K and K' valleys) of the hexagonal Brillouin zone of a MoSe₂/WSe₂ heterostructure, with the twist angle of 60-degree. The K and K' valleys at the conduction band minimum (in MoSe₂) and valence band maximum (in WSe₂) are aligned in momentum space. Here α and β are the heterostructure valleys, and red color stands for spin up, blue color stands for spin down.

(d) Configurations of the interlayer exciton at α and β valleys. Solid dots represent the electrons and the empty ones represent the holes. The dashed lines indicate the formation of triplet interlayer exciton (IX_T) and the singlet interlayer exciton (IX_S), where green (purple) color represents σ^+ (σ^-) helicity PL observed experimentally.

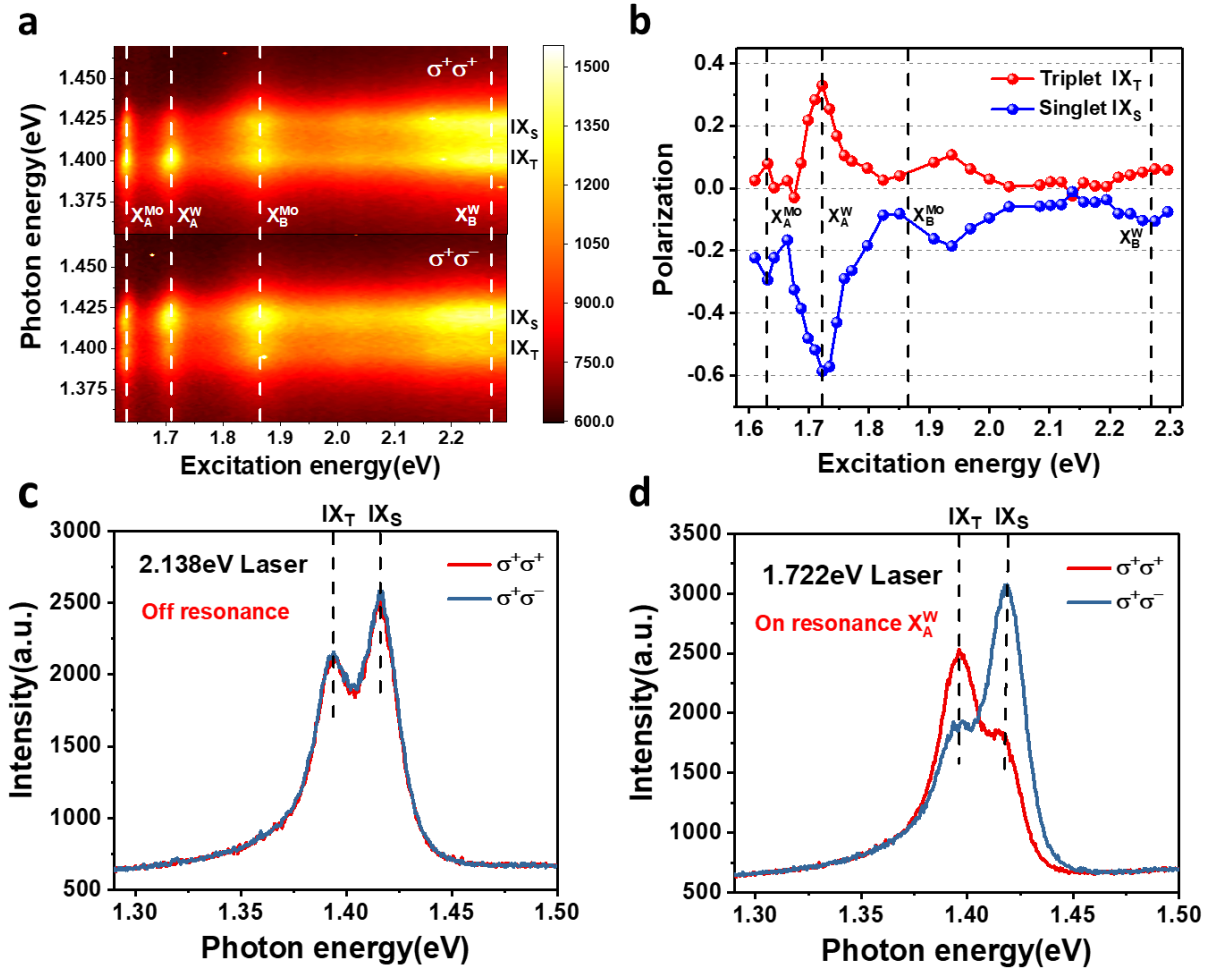


Figure 3. PLE spectra of interlayer excitons at 77 K. (a) Color plot of the PL spectra of interlayer exciton as a function of excitation photon energy. X_B^W , X_B^{Mo} , X_A^W , X_A^{Mo} correspond to the photon energy of WSe₂ B exciton, MoSe₂ B exciton, WSe₂ A exciton and MoSe₂ A exciton modes, respectively. The PL measurement uses circularly polarized light (σ^+) for excitation and detects PL with the same (σ^+) or opposite (σ^-) helicity. (b) Valley polarization of two interlayer exciton states as a function of excitation energy. (c) PL spectra of interlayer exciton excited off-resonance, with the excitation photon energy centered at 2.138 eV. (d) PL spectra of interlayer exciton excited resonantly at WSe₂ A exciton energy (1.722 eV).

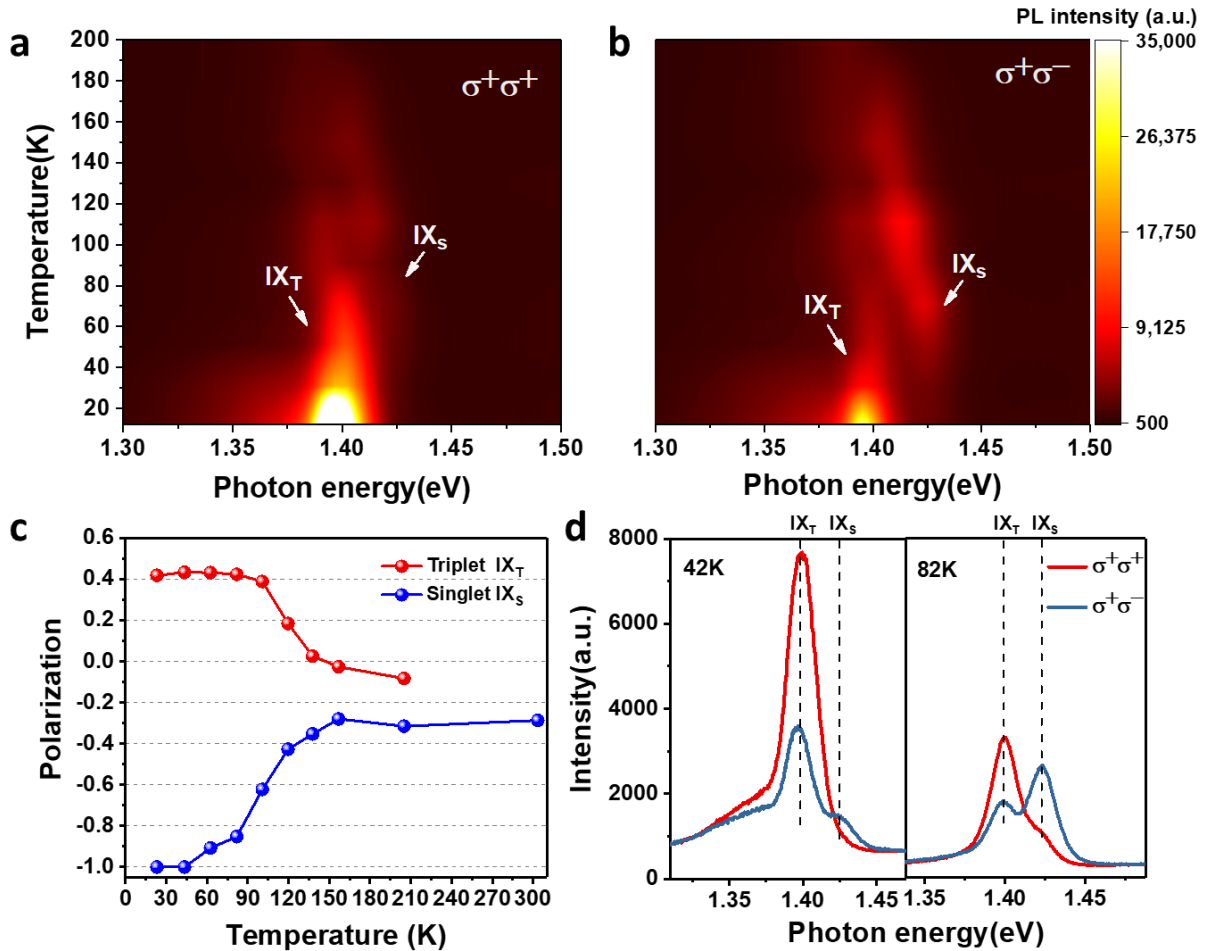


Figure 4. Temperature-dependent valley polarization of interlayer excitons. (a) and (b) are color plots of the PL spectra of interlayer exciton as a function of temperature in $\sigma^+\sigma^+$ and $\sigma^+\sigma^-$ configuration, respectively. (c) Valley polarization of two interlayer exciton states as a function of temperature. (d) Representative PL spectra of interlayer exciton at 42 K and 82 K.

REFERENCES

- (1) Mak, K. F.; He, K.; Lee, C.; Lee, G. H.; Hone, J.; Heinz, T. F.; Shan, J. Tightly Bound Triions in Monolayer MoS₂. *Nat. Mater.* **2012**, *12*, 207–211.
- (2) Ross, J. S.; Wu, S.; Yu, H.; Ghimire, N. J.; Jones, A. M.; Aivazian, G.; Yan, J.; Mandrus, D. G.; Xiao, D.; Yao, W.; Xu, X. Electrical Control of Neutral and Charged Excitons in a Monolayer Semiconductor. *Nat. Commun.* **2013**, *4*, 1474.

- (3) Zhu, B.; Chen, X.; Cui, X. Exciton Binding Energy of Monolayer WS₂. *Sci. Rep.* **2015**, *5*, 9218.
- (4) Gerd, P.; Philipp, N.; Julia, K.; Nicola, P.; Christoph, S.; Christian, S.; Tobias, K. Identification of Excitons, Trions and Biexcitons in Single-Layer WS₂. *Phys. status solidi (RRL)-Rapid Res. Lett.* **2015**, *9*, 457–461.
- (5) Singh, A.; Moody, G.; Wu, S.; Wu, Y.; Ghimire, N. J.; Yan, J.; Mandrus, D. G.; Xu, X.; Li, X. Coherent Electronic Coupling in Atomically Thin MoS₂. *Phys. Rev. Lett.* **2014**, *112*, 216804.
- (6) Li, Z.; Wang, T.; Lu, Z.; Jin, C.; Chen, Y.; Meng, Y.; Lian, Z.; Taniguchi, T.; Watanabe, K.; Zhang, S.; Smirnov, D.; Shi, S.-F. Revealing the Biexciton and Trion-Exciton Complexes in BN Encapsulated WSe₂. *Nat. Commun.* **2018**, *9*, 3719.
- (7) Yu, Y.; Hu, S.; Su, L.; Huang, L.; Liu, Y.; Jin, Z.; Purezky, A. A.; Geohegan, D. B.; Kim, K. W.; Zhang, Y.; Cao, L. Equally Efficient Interlayer Exciton Relaxation and Improved Absorption in Epitaxial and Nonepitaxial MoS₂/WS₂ Heterostructures. *Nano Lett.* **2015**, *15*, 486–491.
- (8) Rigosi, A. F.; Hill, H. M.; Li, Y.; Chernikov, A.; Heinz, T. F. Probing Interlayer Interactions in Transition Metal Dichalcogenide Heterostructures by Optical Spectroscopy: MoS₂/WS₂ and MoSe₂/WSe₂. *Nano Lett.* **2015**, *15*, 5033–5038.
- (9) Cheng, R.; Li, D.; Zhou, H.; Wang, C.; Yin, A.; Jiang, S.; Liu, Y.; Chen, Y.; Huang, Y.; Duan, X. Electroluminescence and Photocurrent Generation from Atomically Sharp WSe₂/MoS₂ Heterojunction p–n Diodes. *Nano Lett.* **2014**, *14*, 5590–5597.
- (10) Lee, C.-H.; Lee, G.-H.; van der Zande, A. M.; Chen, W.; Li, Y.; Han, M.; Cui, X.; Arefe, G.; Nuckolls, C.; Heinz, T. F.; Guo, J.; Hone, J.; Kim, P. Atomically Thin P–n Junctions with van Der Waals Heterointerfaces. *Nat. Nanotechnol.* **2014**, *9*, 676–681.
- (11) Klots, A. R.; Newaz, A. K. M.; Wang, B.; Prasai, D.; Krzyzanowska, H.; Lin, J.; Caudel, D.; Ghimire, N. J.; Yan, J.; Ivanov, B. L.; Velizhanin, K. A.; Burger, A.; Mandrus, D. G.; Tolk, N. H.; Pantelides, S. T.; Bolotin, K. I. Probing Excitonic States in Suspended Two-Dimensional Semiconductors by Photocurrent Spectroscopy. *Sci. Rep.* **2014**, *4*, 6608.
- (12) Fang, H.; Battaglia, C.; Carraro, C.; Nemsak, S.; Ozdol, B.; Kang, J. S.; Bechtel, H. A.; Desai, S. B.; Kronast, F.; Unal, A. A.; Conti, G.; Conlon, C.; Palsson, G. K.; Martin, M. C.; Minor, A. M.; Fadley, C. S.; Yablonovitch, E.; Maboudian, R.; Javey, A. Strong Interlayer Coupling in van Der Waals Heterostructures Built from Single-Layer Chalcogenides. *Proc. Natl. Acad. Sci.* **2014**, *111*, 6198–6202.
- (13) Jin, C.; Ma, E. Y.; Karni, O.; Regan, E. C.; Wang, F.; Heinz, T. F. Ultrafast Dynamics in van Der Waals Heterostructures. *Nat. Nanotechnol.* **2018**, *13*, 994–1003.

- (14) Rivera, P.; Yu, H.; Seyler, K. L.; Wilson, N. P.; Yao, W.; Xu, X. Interlayer Valley Excitons in Heterobilayers of Transition Metal Dichalcogenides. *Nat. Nanotechnol.* **2018**, *13*, 1004–1015.
- (15) Kunstmann, J.; Mooshammer, F.; Nagler, P.; Chaves, A.; Stein, F.; Paradiso, N.; Plechinger, G.; Strunk, C.; Schüller, C.; Seifert, G.; Reichman, D. R.; Korn, T. Momentum-Space Indirect Interlayer Excitons in Transition-Metal Dichalcogenide van Der Waals Heterostructures. *Nat. Phys.* **2018**, *14*, 801–805.
- (16) Zhang, J.; Wang, J.; Chen, P.; Sun, Y.; Wu, S.; Jia, Z.; Lu, X.; Yu, H.; Chen, W.; Zhu, J.; Xie, G.; Yang, R.; Shi, D.; Xu, X.; Xiang, J.; Liu, K.; Zhang, G. Observation of Strong Interlayer Coupling in MoS₂/WS₂ Heterostructures. *Adv. Mater.* **2016**, *28*, 1950–1956.
- (17) Palummo, M.; Bernardi, M.; Grossman, J. C. Exciton Radiative Lifetimes in Two-Dimensional Transition Metal Dichalcogenides. *Nano Lett.* **2015**, *15*, 2794–2800.
- (18) Ross, J. S.; Rivera, P.; Schaibley, J.; Lee-Wong, E.; Yu, H.; Taniguchi, T.; Watanabe, K.; Yan, J.; Mandrus, D.; Cobden, D.; Yao, W.; Xu, X. Interlayer Exciton Optoelectronics in a 2D Heterostructure p–n Junction. *Nano Lett.* **2017**, *17*, 638–643.
- (19) Baranowski, M.; Surrente, A.; Klopotoski, L.; Urban, J. M.; Zhang, N.; Maude, D. K.; Wiwatowski, K.; Mackowski, S.; Kung, Y. C.; Dumcenco, D.; Kis, A.; Plochocka, P. Probing the Interlayer Exciton Physics in a MoS₂/MoSe₂/MoS₂ van Der Waals Heterostructure. *Nano Lett.* **2017**, *17*, 6360–6365.
- (20) Rivera, P.; Schaibley, J. R.; Jones, A. M.; Ross, J. S.; Wu, S.; Aivazian, G.; Klement, P.; Seyler, K.; Clark, G.; Ghimire, N. J.; Yan, J.; Mandrus, D. G.; Yao, W.; Xu, X. Observation of Long-Lived Interlayer Excitons in Monolayer MoSe₂–WSe₂ Heterostructures. *Nat. Commun.* **2015**, *6*, 6242.
- (21) Miller, B.; Steinhoff, A.; Pano, B.; Klein, J.; Jahnke, F.; Holleitner, A.; Wurstbauer, U. Long-Lived Direct and Indirect Interlayer Excitons in van Der Waals Heterostructures. *Nano Lett.* **2017**, *17*, 5229–5237.
- (22) Nagler, P.; Plechinger, G.; Ballottin, M. V.; Mitioglu, A.; Meier, S.; Paradiso, N.; Strunk, C.; Chernikov, A.; Christianen, P. C. M.; Schüller, C.; Korn, T. Interlayer Exciton Dynamics in a Dichalcogenide Monolayer Heterostructure. *2D Mater.* **2017**, *4*, 25112.
- (23) Yu, H.; Liu, G. Bin; Yao, W. Brightened Spin-Triplet Interlayer Excitons and Optical Selection Rules in van Der Waals Heterobilayers. *2D Mater.* **2018**, *5*, 035021.
- (24) Kormányos, A.; Zólyomi, V.; Drummond, N. D.; Burkard, G. Spin-Orbit Coupling, Quantum Dots, and Qubits in Monolayer Transition Metal Dichalcogenides. *Phys. Rev. X* **2014**, *4*, 039901.
- (25) Wang, G.; Robert, C.; Suslu, A.; Chen, B.; Yang, S.; Alamdari, S.; Gerber, I. C.; Amand, T.; Marie, X.; Tongay, S.; Urbaszek, B. Spin-Orbit Engineering in

- Transition Metal Dichalcogenide Alloy Monolayers. *Nat. Commun.* **2015**, *6*, 10110.
- (26) Macneill, D.; Heikes, C.; Mak, K. F.; Anderson, Z.; Kormányos, A.; Zólyomi, V.; Park, J.; Ralph, D. C. Breaking of Valley Degeneracy by Magnetic Field in Monolayer MoSe₂. *Phys. Rev. Lett.* **2015**, *114*, 037401.
- (27) Aivazian, G.; Gong, Z.; Jones, A. M.; Chu, R.-L.; Yan, J.; Mandrus, D. G.; Zhang, C.; Cobden, D.; Yao, W.; Xu, X. Magnetic Control of Valley Pseudospin in Monolayer WSe₂. *Nat. Phys.* **2015**, *11*, 148–152.
- (28) Li, Y.; Ludwig, J.; Low, T.; Chernikov, A.; Cui, X.; Arefe, G.; Kim, Y. D.; Van Der Zande, A. M.; Rigosi, A.; Hill, H. M.; Kim, S. H.; Hone, J.; Li, Z.; Smirnov, D.; Heinz, T. F. Valley Splitting and Polarization by the Zeeman Effect in Monolayer MoSe₂. *Phys. Rev. Lett.* **2014**, *113*, 266804.
- (29) Srivastava, A.; Sidler, M.; Allain, A. V.; Lembke, D. S.; Kis, A.; Imamoglu, A. Valley Zeeman Effect in Elementary Optical Excitations of Monolayer WSe₂. *Nat. Phys.* **2015**, *11*, 141–147.
- (30) Zhang, X. X.; You, Y.; Zhao, S. Y. F.; Heinz, T. F. Experimental Evidence for Dark Excitons in Monolayer WSe₂. *Phys. Rev. Lett.* **2015**, *115*, 257403.
- (31) Zhang, X. X.; Cao, T.; Lu, Z.; Lin, Y. C.; Zhang, F.; Wang, Y.; Li, Z.; Hone, J. C.; Robinson, J. A.; Smirnov, D.; Louie, S. G.; Heinz, T. F. Magnetic Brightening and Control of Dark Excitons in Monolayer WSe₂. *Nat. Nanotechnol.* **2017**, *12*, 883–888.
- (32) Deilmann, T.; Thygesen, K. S. Dark Excitations in Monolayer Transition Metal Dichalcogenides. *Phys. Rev. B* **2017**, *96*, 201113.
- (33) Koperski, M.; Molas, M. R.; Arora, A.; Nogajewski, K.; Bartos, M.; Wyzula, J.; Vaclavkova, D.; Kossacki, P.; Potemski, M. Orbital, Spin and Valley Contributions to Zeeman Splitting of Excitonic Resonances in MoSe₂, WSe₂ and WS₂ Monolayers. *2D Mater.* **2018**, *6*, 15001.
- (34) Zhang, L.; Gogna, R.; Burg, G. W.; Horng, J.; Paik, E.; Chou, Y.-H.; Kim, K.; Tutuc, E.; Deng, H. Highly Valley-Polarized Singlet and Triplet Interlayer Excitons in van Der Waals Heterostructure. *Phys. Rev. B* **2019**, *100*, 041402.
- (35) Jiang, C.; Xu, W.; Rasmita, A.; Huang, Z.; Li, K.; Xiong, Q.; Gao, W. Microsecond Dark-Exciton Valley Polarization Memory in Two-Dimensional Heterostructures. *Nat. Commun.* **2018**, *9*, 753.
- (36) Rivera, P.; Seyler, K. L.; Yu, H.; Schaibley, J. R.; Yan, J.; Mandrus, D. G.; Yao, W.; Xu, X. Valley-Polarized Exciton Dynamics in a 2D Semiconductor Heterostructure. *Science*. **2016**, *351*, 688–691.
- (37) Yu, H.; Wang, Y.; Tong, Q.; Xu, X.; Yao, W. Anomalous Light Cones and Valley Optical Selection Rules of Interlayer Excitons in Twisted Heterobilayers. *Phys. Rev. Lett.* **2015**, *115*, 187002.

- (38) Hanbicki, A. T.; Chuang, H. J.; Rosenberger, M. R.; Hellberg, C. S.; Sivaram, S. V.; McCreary, K. M.; Mazin, I. I.; Jonker, B. T. Double Indirect Interlayer Exciton in a $\text{MoSe}_2/\text{WSe}_2$ van Der Waals Heterostructure. *ACS Nano* **2018**, *12*, 4719–4726.
- (39) Hsu, W. T.; Lu, L. S.; Wu, P. H.; Lee, M. H.; Chen, P. J.; Wu, P. Y.; Chou, Y. C.; Jeng, H. T.; Li, L. J.; Chu, M. W.; Chang, W. H. Negative Circular Polarization Emissions from $\text{WSe}_2/\text{MoSe}_2$ Commensurate Heterobilayers. *Nat. Commun.* **2018**, *9*, 1356.
- (40) Ciarrocchi, A.; Unuchek, D.; Avsar, A.; Watanabe, K.; Taniguchi, T.; Kis, A. Polarization Switching and Electrical Control of Interlayer Excitons in Two-Dimensional van Der Waals Heterostructures. *Nat. Photonics* **2019**, *13*, 131–136.
- (41) Seyler, K. L.; Rivera, P.; Yu, H.; Wilson, N. P.; Ray, E. L.; Mandrus, D. G.; Yan, J.; Yao, W.; Xu, X. Signatures of Moiré-Trapped Valley Excitons in $\text{MoSe}_2/\text{WSe}_2$ Heterobilayers. *Nature* **2019**, *567*, 66–70.
- (42) Tran, K.; Moody, G.; Wu, F.; Lu, X.; Choi, J.; Kim, K.; Rai, A.; Sanchez, D. A.; Quan, J.; Singh, A.; Embley, J.; Zepeda, A.; Campbell, M.; Autry, T.; Taniguchi, T.; Watanabe, K.; Lu, N.; Banerjee, S. K.; Silverman, K. L.; Kim, S. Evidence for Moiré Excitons in van Der Waals Heterostructures. *Nature* **2019**, *567*, 71–75.
- (43) Alexeev, E. M.; Ruiz-Tijerina, D. A.; Danovich, M.; Hamer, M. J.; Terry, D. J.; Nayak, P. K.; Ahn, S.; Pak, S.; Lee, J.; Sohn, J. I.; Molas, M. R.; Koperski, M.; Watanabe, K.; Taniguchi, T.; Novoselov, K. S.; Gorbachev, R. V.; Shin, H. S.; Fal'ko, V. I.; Tartakovskii, A. I. Resonantly Hybridized Excitons in Moiré Superlattices in van Der Waals Heterostructures. *Nature* **2019**, *567*, 81–86.
- (44) Jin, C.; Regan, E. C.; Yan, A.; Iqbal Bakti Utama, M.; Wang, D.; Zhao, S.; Qin, Y.; Yang, S.; Zheng, Z.; Shi, S.; Watanabe, K.; Taniguchi, T.; Tongay, S.; Zettl, A.; Wang, F. Observation of Moiré Excitons in WSe_2/WS_2 Heterostructure Superlattices. *Nature* **2019**, *567*, 76–80.
- (45) Jin, C.; Regan, E. C.; Wang, D.; Iqbal Bakti Utama, M.; Yang, C.-S.; Cain, J.; Qin, Y.; Shen, Y.; Zheng, Z.; Watanabe, K.; Taniguchi, T.; Tongay, S.; Zettl, A.; Wang, F. Identification of Spin, Valley and Moiré Quasi-Angular Momentum of Interlayer Excitons. *Nat. Phys.* **2019**.
- (46) Zhang, N.; Surrente, A.; Baranowski, M.; Maude, D. K.; Gant, P.; Castellanos-Gomez, A.; Plochocka, P. Moiré Intralayer Excitons in a $\text{MoSe}_2/\text{MoS}_2$ Heterostructure. *Nano Lett.* **2018**, *18*, 7651–7657.
- (47) Rybkovskiy, D. V.; Gerber, I. C.; Durnev, M. V. Atomically Inspired $k \cdot p$ Approach and Valley Zeeman Effect in Transition Metal Dichalcogenide Monolayers. *Phys. Rev. B* **2017**, *95*, 155406.
- (48) Wang, G.; Bouet, L.; Glazov, M. M.; Amand, T.; Ivchenko, E. L.; Palleau, E.; Marie, X.; Urbaszek, B. Magneto-Optics in Transition Metal Diselenide Monolayers. *2D Mater.* **2015**, *2*, 034002.

- (49) Li, Z.; Wang, T.; Jin, C.; Lu, Z.; Lian, Z.; Meng, Y.; Blei, M.; Gao, S.; Taniguchi, T.; Watanabe, K.; Ren, T.; Tongay, S.; Yang, L.; Smirnov, D.; Cao, T.; Shi, S. F. Emerging Photoluminescence from the Dark-Exciton Phonon Replica in Monolayer WSe₂. *Nat. Commun.* **2019**, *10*, 2469.
- (50) Nagler, P.; Ballottin, M. V.; Mitioglu, A. A.; Mooshammer, F.; Paradiso, N.; Strunk, C.; Huber, R.; Chernikov, A.; Christianen, P. C. M.; Schüller, C.; Korn, T. Giant Zeeman Splitting Inducing Near-Unity Valley Polarization in van Der Waals Heterostructures. *Nat. Commun.* **2017**, *8*, 1551.
- (51) Kim, J.; Jin, C.; Chen, B.; Cai, H.; Zhao, T.; Lee, P.; Kahn, S.; Watanabe, K.; Taniguchi, T.; Tongay, S.; Crommie, M. F.; Wang, F. Observation of Ultralong Valley Lifetime in WSe₂/MoS₂ Heterostructures. *Sci. Adv.* **2017**, *3*, e1700518.
- (52) Schaibley, J. R.; Rivera, P.; Yu, H.; Seyler, K. L.; Yan, J.; Mandrus, D. G.; Taniguchi, T.; Watanabe, K.; Yao, W.; Xu, X. Directional Interlayer Spin-Valley Transfer in Two-Dimensional Heterostructures. *Nat. Commun.* **2016**, *7*, 13747.
- (53) Hsu, W. T.; Chen, Y. L.; Chen, C. H.; Liu, P. S.; Hou, T. H.; Li, L. J.; Chang, W. H. Optically Initialized Robust Valley-Polarized Holes in Monolayer WSe₂. *Nat. Commun.* **2015**, *6*, 8963.
- (54) Li, Y.; Wang, T.; Wang, H.; Li, Z.; Chen, Y.; West, D.; Sankar, R.; Ulaganathan, R. K.; Chou, F.; Wetzel, C.; Xu, C. Y.; Zhang, S.; Shi, S. F. Enhanced Light Emission from the Ridge of Two-Dimensional InSe Flakes. *Nano Lett.* **2018**, *18*, 5078–5084.
- (55) Empedocles, S. A.; Bawendi, M. G. Quantum-Confined Stark Effect in Single CdSe Nanocrystallite Quantum Dots. *Science.* **1997**, *278*, 2114–2117.
- (56) Koperski, M.; Molas, M. R.; Arora, A.; Nogajewski, K.; Slobodeniuk, A. O.; Faugeras, C.; Potemski, M. Optical Properties of Atomically Thin Transition Metal Dichalcogenides: Observations and Puzzles. *Nanophotonics* **2017**, *6*, 1289.
- (57) Xiao, D.; Yao, W.; Niu, Q. Valley-Contrasting Physics in Graphene: Magnetic Moment and Topological Transport. *Phys. Rev. Lett.* **2007**, *99*, 236809.
- (58) Slobodeniuk, A. O.; Bala, Ł.; Koperski, M.; Molas, M. R.; Kossacki, P.; Nogajewski, K.; Bartos, M.; Watanabe, K.; Taniguchi, T.; Faugeras, C.; Potemski, M. Fine Structure of K-Excitons in Multilayers of Transition Metal Dichalcogenides. *2D Mater.* **2019**, *6*, 25026.
- (59) Liu, G. Bin; Shan, W. Y.; Yao, Y.; Yao, W.; Xiao, D. Three-Band Tight-Binding Model for Monolayers of Group-VIB Transition Metal Dichalcogenides. *Phys. Rev. B* **2013**, *88*, 085433.
- (60) Xiao, D.; Liu, G. Bin; Feng, W.; Xu, X.; Yao, W. Coupled Spin and Valley Physics in Monolayers of MoS₂ and Other Group-VI Dichalcogenides. *Phys. Rev. Lett.* **2012**, *108*, 196802.
- (61) Tang, Y.; Mak, K. F.; Shan, J. Long Valley Lifetime of Dark Excitons in Single-Layer WSe₂. *Nat. Commun.* **2019**, *10*, 4047.

- (62) Malic, E.; Selig, M.; Feierabend, M.; Brem, S.; Christiansen, D.; Wendler, F.; Knorr, A.; Berghäuser, G. Dark Excitons in Transition Metal Dichalcogenides. *Phys. Rev. Mater.* **2018**, *2*, 14002.
- (63) Park, K. D.; Jiang, T.; Clark, G.; Xu, X.; Raschke, M. B. Radiative Control of Dark Excitons at Room Temperature by Nano-Optical Antenna-Tip Purcell Effect. *Nat. Nanotechnol.* **2018**, *13*, 59–64.
- (64) Wang, G.; Robert, C.; Glazov, M. M.; Cadiz, F.; Courtade, E.; Amand, T.; Lagarde, D.; Taniguchi, T.; Watanabe, K.; Urbaszek, B.; Marie, X. In-Plane Propagation of Light in Transition Metal Dichalcogenide Monolayers: Optical Selection Rules. *Phys. Rev. Lett.* **2017**, *119*, 047401.
- (65) Li, Z.; Wang, T.; Lu, Z.; Khatoniari, M.; Lian, Z.; Meng, Y.; Blei, M.; Taniguchi, T.; Watanabe, K.; McGill, S. A.; Tongay, S.; Menon, V. M.; Smirnov, D.; Shi, S.-F. Direct Observation of Gate-Tunable Dark Trions in Monolayer WSe₂. *Nano Lett.* **2019**, *19*, 6886–6893.
- (66) Ji, Z.; Hong, H.; Zhang, J.; Zhang, Q.; Huang, W.; Cao, T.; Qiao, R.; Liu, C.; Liang, J.; Jin, C.; Jiao, L.; Shi, K.; Meng, S.; Liu, K. Robust Stacking-Independent Ultrafast Charge Transfer in MoS₂/WS₂ Bilayers. *ACS Nano* **2017**, *11*, 12020–12026.
- (67) Wang, H.; Bang, J.; Sun, Y.; Liang, L.; West, D.; Meunier, V.; Zhang, S. The Role of Collective Motion in the Ultrafast Charge Transfer in van Der Waals Heterostructures. *Nat. Commun.* **2016**, *7*, 11504.
- (68) Zhu, X.; Monahan, N. R.; Gong, Z.; Zhu, H.; Williams, K. W.; Nelson, C. A. Charge Transfer Excitons at van Der Waals Interfaces. *J. Am. Chem. Soc.* **2015**, *137*, 8313–8320.
- (69) Hong, X.; Kim, J.; Shi, S.-F.; Zhang, Y.; Jin, C.; Sun, Y.; Tongay, S.; Wu, J.; Zhang, Y.; Wang, F. Ultrafast Charge Transfer in Atomically Thin MoS₂/WS₂ Heterostructures. *Nat. Nanotechnol.* **2014**, *9*, 682.
- (70) Norden, T.; Zhao, C.; Zhang, P.; Sabirianov, R.; Petrou, A.; Zeng, H. Giant Valley Splitting in Monolayer WS₂ by Magnetic Proximity Effect. *Nat. Commun.* **2019**, *10*, 4163.
- (71) Tong, Q.; Chen, M.; Yao, W. Magnetic Proximity Effect in a van Der Waals Moiré Superlattice. *Phys. Rev. Appl.* **2019**, *12*, 24031.
- (72) Zollner, K.; Faria Junior, P. E.; Fabian, J. Proximity Exchange Effects in MoSe₂ and WSe₂ Heterostructures with CrI₃: Twist Angle, Layer, and Gate Dependence. *Phys. Rev. B* **2019**, *100*, 085128.
- (73) Shayan, K.; Liu, N.; Cupo, A.; Ma, Y.; Luo, Y.; Meunier, V.; Strauf, S. Magnetic Proximity Coupling of Quantum Emitters in WSe₂ to van Der Waals Ferromagnets. *Nano Lett.* **2019**, *19*, 7301–7308.
- (74) Seyler, K. L.; Zhong, D.; Huang, B.; Linpeng, X.; Wilson, N. P.; Taniguchi, T.; Watanabe, K.; Yao, W.; Xiao, D.; McGuire, M. A.; Fu, K.-M. C.; Xu, X. Valley

Manipulation by Optically Tuning the Magnetic Proximity Effect in WSe₂/CrI₃ Heterostructures. *Nano Lett.* **2018**, *18*, 3823–3828.

- (75) Zhao, C.; Norden, T.; Zhang, P.; Zhao, P.; Cheng, Y.; Sun, F.; Parry, J. P.; Taheri, P.; Wang, J.; Yang, Y.; Scrace, T.; Kang, K.; Yang, S.; Miao, G.; Sabirianov, R.; Kioseoglou, G.; Huang, W.; Petrou, A.; Zeng, H. Enhanced Valley Splitting in Monolayer WSe₂ Due to Magnetic Exchange Field. *Nat. Nanotechnol.* **2017**, *12*, 757–762.

TOC

